

The effect of multi-component aerosol particles on quantitative laser-induced breakdown spectroscopy: Consideration of localized matrix effects[☆]

P.K. Diwakar, P.B. Jackson, D.W. Hahn^{*}

Department of Mechanical and Aerospace Engineering, University of Florida, Gainesville, FL 32611-6300, United States

Received 19 December 2006; accepted 2 October 2007

Available online 9 October 2007

Abstract

Spectral measurements were performed in a laser-induced plasma to assess the changes in sodium or magnesium analyte emission response from particle-derived sources with the addition of concomitant mass to the aerosol particles. Temporally resolved measurements revealed up to a 50% enhancement in analyte emission with the addition of the elements copper, zinc or tungsten at mass ratios from 1:9 to 1:19, although the enhancement generally diminished by delay times of 60 μ s. Additional measurements in magnesium–cadmium aerosol particles were performed to assess the temporal profile of plasma temperature in the spatial vicinity of the aerosol particles using the ion-to-neutral emission ratios. These measurements revealed a general increase in localized plasma temperature with increasing delay time, which is attributed with an initial suppression of plasma temperature about the aerosol particles as plasma energy is required to vaporize and ionize the aerosol particle mass. These measurements provide direct evidence of a matrix effect for aerosol particles, which is attributed primarily to perturbations in the localized plasma properties. These perturbations are minimized at longer plasma delay times; hence quantitative LIBS analysis of aerosol particles should be performed with careful attention given to the temporal plasma evolution. The data further elucidate the complex interactions between the plasma gas and the aerosol particles, during which the finite time-scales of particle dissociation, and heat and mass transfer are equally important.

© 2007 Elsevier B.V. All rights reserved.

Keywords: Laser-induced plasma spectroscopy; LIBS; Fractionation; Matrix effects; Aerosol analysis

1. Introduction

Laser-induced breakdown spectroscopy (LIBS) is an atomic emission spectroscopic technique that has been widely used for elemental analysis of solid, gaseous, and aerosol samples [1–2]. Generally all elements can be analyzed by this technique, while the relative ease of sample preparation provides an advantage as compared to many other techniques. The LIBS technique involves a high energy, pulsed laser beam focused onto the sample to create a high temperature plasma wherein the sample is dissociated into atoms and ions. The subsequent atomic emission from the plasma becomes the analytical signal through which the elemental composition of the desired analyte can be

determined. Both qualitative and quantitative analyses are possible using LIBS. While for qualitative analysis LIBS is a very robust technique, for quantitative analysis several issues remain the focus of contemporary research. One such issue for quantitative analysis is the nature of the plasma–analyte interaction and the potential for matrix effects. While matrix effects have received considerable attention over the years with regard to LIBS and other analytical techniques, the unique application of LIBS for aerosol analysis has been largely unexplored with regard to this topic. The current study is limited to the implementation of LIBS for analysis of aerosol systems, namely gas-phase breakdown in the presence of fine particles.

Precise calibration of the analyte spectral signal with respect to the true analyte concentration within a laser-induced plasma is necessary for achieving accurate results with the LIBS technique. A key assumption for LIBS is that the sample composition remains the same in the plasma plume, as complete dissociation of the constituent species within the laser-induced plasma results in independence of the analyte atomic emission signal on the analyte

[☆] This paper was presented at the 4th International Conference on Laser Induced Plasma Spectroscopy and Applications (LIBS 2006) held in Montreal, Canada, 5–8 September 2006, and is published in the Special Issue of Spectrochimica Acta Part B, dedicated to that conference.

^{*} Corresponding author.

E-mail address: dwhahn@ufl.edu (D.W. Hahn).

source, as well as independence with respect to the presence of other elements. However, recent work by Hohreiter and Hahn has demonstrated that individual aerosol particles dissociate over a finite time scale of some microseconds, and that finite atomic diffusion rates for particle-derived atoms result in the atoms being localized about the original particle location over these same time scales [3]. This behavior suggests that aerosol particle-derived analytes may very well experience different plasma conditions (i.e. temperature and free electron density) than the overall average (i.e. bulk) plasma conditions, which may in turn induce matrix conditions not previously considered in the idealized model of analyte independence. This effect of variation of analyte response by different elements within the original bulk material matrix is referred to as fractionation or matrix effects, and has been widely observed and studied in another spectroscopic techniques such as inductively-coupled plasma atomic emission spectroscopy (ICP-AES), and laser ablation inductively-coupled plasma mass spectrometry (LA-ICP-MS). Fractionation or matrix effects render analytical techniques less effective for quantitative analysis.

Various studies have been performed in the analytical community to study and understand fractionation and matrix effects on the resulting analyte response [4–10]. In an effort to correct for matrix effects, a common analytical procedure involves normalization of analyte signal to a standard reference signal, although appropriate reference signals are not always readily available. For example, aerosol particle analysis in ambient air presents a widely varying range of particle composition with no invariant species for signal normalization. Alternatively, acoustic signals and temperature normalization coefficients have been used to calibrate the analyte signal as a means of accounting for vaporized mass and temperature excitation variation, respectively, in the plasma [6]. Along these lines, Mermet suggested the use of robust conditions namely high power, low carrier gas flow rate and medium solvent loading to minimize matrix effects by using the ratio of ionic-to-neutral magnesium atomic emission lines [7].

The LA-ICP-MS technique has become a popular choice for trace elemental analysis of solid samples. With LA-ICP-MS, three sources of fractionation may be considered: during the laser ablation process, during transport to the ICP, and finally within the inductively coupled plasma. Fractionation in the ablation process is attributed to laser-material interaction, and may depend on laser fluence, laser wavelength, and laser pulse width, as well as subsequent analyte transport effects that are related to the resulting size distribution of the aerosol (including nucleation effects), carrier gases, and transport losses due to impaction and diffusion losses [10–17]. Such effects are largely eliminated with direct aerosol sampling via LIBS, as implemented in the current study. More relevant to LIBS analysis is fractionation within the inductively-coupled plasma, which can be attributed to incomplete vaporization, atomization, and ionization processes. These processes are highly dependent on the plasma temperature (both gas temperature and electron temperature) and the free electron density [7,18–20].

Budic reported the suppression of analyte emission with ICP-AES in the presence of matrix elements, which was attributed to a shift in ionization equilibrium [21]. Gunther et al. have

demonstrated that incomplete vaporization of large particles in the ICP (1–1.5 μm) causes elemental fractionation effects in LA-ICP-MS [5]. Significantly, even after optimizing the LA-ICP-MS system for minimization of ablation and transport effects, they found differing analyte responses that were related to the overall particle size entering the ICP, concluding that plasma-particle processes play a major role in analyte response. Detailed study has been done by Olesik investigating the vaporization process and kinetics of droplets in ICP-MS, with a focus on matrix effects [22]. In more recent work, Wang et al. showed that vaporization efficiency and subsequent radial diffusion are controlling processes that are coupled closely to the plasma gas temperature [4]. While increased plasma temperature can increase particle vaporization, a careful balance must be given to a concomitant increase in atomic diffusion, which can result in an increased analyte fraction missing the MS skimmer.

As related in the above comments, the roles of particle vaporization, dissociation, ionization, and diffusion are common to a range of analytical techniques, notably the direct analysis of aerosol particles with LIBS and LA-ICP-MS. Previous studies have demonstrated the laser-induced plasma robustness to aerosol sampling, including breakdown initiation and plasma temperature and electron density [23,24]. However, our more recent work has shown that plasma-particle interactions are confined to localized regions about the particles, thereby clarifying the differences between bulk plasma properties (which have been shown to be independent of the presence of aerosol particles) and plasma conditions in the immediate vicinity of individual aerosol particles [3]. Olesik showed that localized, incomplete desolvation of aerosol droplets affected average time integrated emission intensity [22]. With this framework in mind, it becomes apparent that small amounts of analyte contained in submicron and micron-sized particles can bring about changes in *localized* plasma temperature, electron density, and ionization fractions, thereby affecting the analyte response. It is the goal of the present study to further understand how particles may perturb the local plasma conditions, and how such perturbations may result in a particle-matrix dependent analyte response with LIBS-based aerosol analysis.

2. Experimental methods

The experimental system for the current study is shown schematically in Fig. 1. For all experiments, a Q-switched Nd:YAG laser (Big Sky CFR 400) operating at the fundamental wavelength (2–5 Hz repetition rate, ~ 20 ns pulse width and 260 mJ/pulse) was used to create the plasma using a 50-mm diameter, 75-mm focal length lens. The plasma emission was collected on axis with the incident laser beam using a pierced mirror and 75-mm focal length condensing lens. The plasma emission was then fiber-coupled (0.22 NA) to a 0.275-m spectrometer (Acton SpectraPro, 2400 groove/mm grating, 0.15-nm resolution). Spectral data were recorded using an intensified CCD detector array. For all experiments, the ICCD was synchronized to the laser Q-switch, and a series of detector delay and integration times were used: 2 μs delay with a 0.4 μs width; 5 μs delay with a 1 μs width; 15 μs delay with a 3 μs width; 25 μs delay with a 5 μs width; 30 μs delay with a 5 μs width; 40 μs

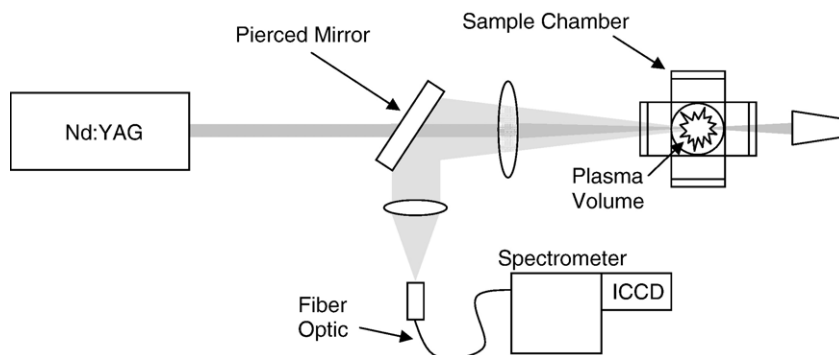


Fig. 1. Top view of experimental apparatus for the LIBS aerosol experiments.

delay with a 8 μs width; and 60 μs delay with a 12 μs width. For each experimental condition, 1000 laser shots were averaged together to produce a representative spectrum, and the measurements were repeated from 5 to 8 times over different days.

2.1. Aerosol generation

All analyte samples flowed through a standard six-way vacuum cross at atmospheric pressure, which functioned as the LIBS sample chamber as previously described [25,26]. A gaseous co-flow of 44 lpm of purified air was used for all experiments. The air was passed through an activated alumina dryer, a coarse particle filter, an additional desiccant dryer, and finally a HEPA filter cartridge prior to entering the sample chamber. All flow rates were controlled with digital mass flow controllers. The aerosol particles were made by nebulizing a solution of the desired analyte at a rate of about 0.15 ml/min using a gas flow of 5 lpm through a pneumatic type nebulizer (Hudson model #1724). All analyte solutions were prepared by diluting ICP-grade analytical standards of 10,000 μg analyte/ml (SPEX CertiPrep) to the desired concentration using ultrapurified deionized water. The solution concentrations were adjusted to provide a nominal range from about 1500 to 25,000 μg analyte/ m^3 through the LIBS sample chamber. Based on previous TEM measurements using the current configuration [25], the average aerosol particle size following droplet desolvation (i.e. solid analyte phase) is expected to be less than 100 nm, while agglomerate formation is considered insignificant. For the current study, analyte species included cadmium, magnesium, and sodium. To verify size and composition for these elements, particles were sampled from the LIBS chamber directly onto carbon-coated 150-mesh copper TEM grids (Electron Microscopy Sciences, FCF150-CU50) and analyzed using TEM (Transmission Electron Microscopy) and EDS (Energy Dispersive Spectroscopy). Overall, the system provided a dispersed, submicron-sized analyte-rich aerosol stream for LIBS analysis.

3. Results and discussion

3.1. Analyte emission enhancement with added aerosol mass

The first set of experiments was performed to assess the change in analyte emission response from an aerosol-derived analyte with the addition of concomitant mass to the aerosol

particles. Specifically, measurements were performed using either sodium or magnesium as the analyte, with either copper, zinc or tungsten used as the concomitant element. Copper, zinc and tungsten were selected due to their range in volatility, noting their corresponding temperatures for a vapor pressure of 10 torr are equal to 1870, 590 and 4490 K, respectively, as compared to 546 K for sodium. For the sodium experiments, solutions of 1000 μg Na/ml were nebulized and the atomic emission of the sodium doublet at 589.00 and 589.59 nm doublet ($0\text{--}16973$ and $0\text{--}16956\text{ cm}^{-1}$) was recorded. The spectral signal was quantified as the peak/base ratio (P/B), where the peak was the integrated full-width intensity while the base was the continuum emission intensity as interpolated using either side of the sodium peaks. The P/B provides a precise emission signal, as it normalizes the atomic signal with plasma continuum emission. The continuum emission near the sodium lines was featureless and rather flat, making peak integration and continuum interpolation straightforward. The experiments were then repeated for solutions of 1000 μg Na/ml with an additional 9000 μg /ml of either Cu, Zn, or W, which corresponds to a Na:Cu, Na:Zn, and Na:W mass ratio of 1:9. For the magnesium experiments, solutions of 500 μg Mg/ml were nebulized and the atomic emission of the magnesium ion at 280.27 nm ($0\text{--}35,669\text{ cm}^{-1}$) and the magnesium neutral at 285.21 nm ($0\text{--}35,051\text{ cm}^{-1}$) were recorded. P/B ratios for the magnesium lines were also calculated in similar way as described for sodium spectra above. The magnesium experiments were then repeated for solutions of 500 μg Mg/ml with an additional 9500 μg /ml of either Zn or W, which corresponds to a Mg:Zn or Mg:W mass ratio of 1:19. For these experiments, TEM and EDS analysis was performed to verify the mean particle size less than 100 nm, and the binary composition of the resulting particles, although detailed quantitative analysis was not performed.

Fig. 2 presents the spectrum corresponding to the pure sodium aerosol particles, along with the spectrum corresponding to the multi-component sodium/copper aerosol particles at the 1:9 mass ratio. Both spectra were recorded at a delay time of 15 μs following plasma initiation. Several interesting features are noted with respect to Fig. 2, namely, that the sodium emission signal is noticeably greater in the sodium–copper aerosol spectrum as compared to the pure sodium aerosol spectrum, despite the constant sodium mass, and that the plasma continuum emission signal is essentially identical for both. One possible reason for the enhancement in Na line intensities can be attributed to the fact that Na is easily ionized,

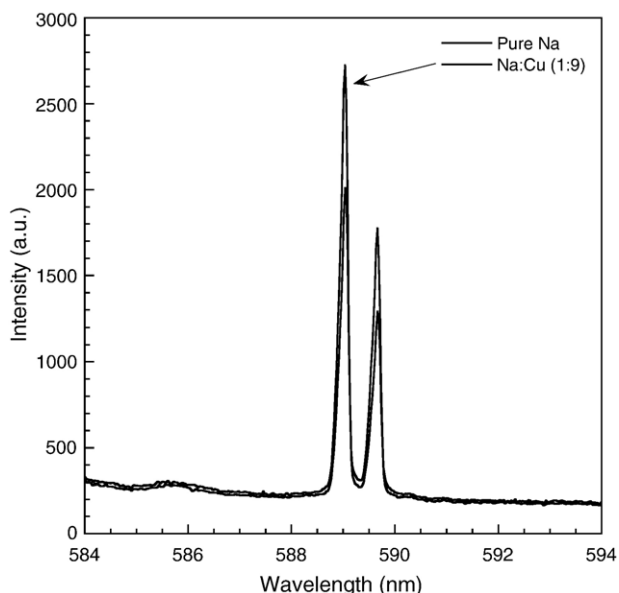


Fig. 2. Sodium emission spectra recorded for pure sodium-based aerosols and for sodium–copper containing aerosols at a 1:9 mass ratio. Spectra were recorded at a time delay of 15 μ s, and are both presented with the same intensity scale.

notably at early stages of plasma development, and therefore the addition of concomitant species may cool down the local plasma volume in the vicinity of the particle, leading to an increase in the Na I-to-Na II ratio. The nearly identical plasma continuum emission intensity was observed for all time delays, and is consistent with previous investigations in which the plasma continuum emission intensity was found to be quite independent of the presence or nature of aerosol particles [24,26,27]. Furthermore, the enhancement in emission of the Na I doublet with additional mass added to the sodium aerosol particles was found to have a temporal dependency. To explore such behavior, the measurements were repeated over the delay times from 2 to 60 μ s following plasma initiation. To quantify these measurements, the sodium signal from the two-component aerosols (either Cu, Zn or W) was normalized to the sodium signal from the pure sodium experiments at each respective delay time. The normalized sodium signal then represents the sodium emission enhancement factor as a function of plasma decay time, with the resulting data presented in Fig. 3. To assess the degree to which the mass ratio of sodium to the concomitant element was important, the sodium/copper measurements were repeated for Na:Cu mass ratios of 1:1, 1:3, and 1:6. Interestingly, the sodium enhancement was rather consistent, with the maximum enhancement factor remaining within 10% of the enhancement factor of 1.53 recorded for the 1:9 mass ratio at a delay of 15 μ s, although a slight trend was seen of decreasing enhancement with decreasing mass ratio. It is important to note here that the actual particle sizes follow a distribution, and that our signal collection strategy (i.e. integrated backscatter) averages over all particle size as well as over all particle locations within the laser-induced plasma. Accordingly, the analytical trend corresponds to an ensemble effect of all particles.

Nearly identical behavior was observed with the magnesium atomic emission signals when comparing the pure magnesium-

based aerosol signal with the magnesium–zinc and magnesium–tungsten aerosol signal. The emission enhancement was observed with both the Mg I and Mg II emission lines. The data for the 285-nm Mg I line are presented in Fig. 4 for the Mg:Zn and Mg:W mass ratio of 1:19. As observed in the figure, the magnesium atomic emission signal was found to be enhanced by the addition of added Zn or W mass, although there was also a significant temporal dependence to this trend similar to the results observed with the sodium aerosol measurements.

The data presented in Figs. 3 and 4 clearly demonstrate an aerosol matrix effect, which is the first time a direct effect of an additional aerosol particle constituent (i.e. Cu, Zn, or W) on an aerosol-derived analyte signal has been documented for LIBS-based aerosol analysis. Radziemski et al. were among the first to perform detailed LIBS-based aerosol measurements using a system with particle sizes estimated to be in the submicron size range [28]. Calibration curves were generated for three analytes, namely cadmium, lead, and zinc, and were characterized by initial linearity followed by various degrees of saturation at higher concentrations, which was attributed to incomplete vaporization of particles. An important finding was the general agreement (within 10%) of lead atomic emission signals of comparable atomic lead concentrations when nebulizing either lead acetate, lead chloride, or lead nitrate. Similar experiments with cadmium revealed a 27% difference in analyte response when comparing nebulized solutions of cadmium nitrate and cadmium chloride. Their study did not explore the effect of the mass of concomitant aerosol elements, therefore, one may not attribute their findings to a particular effect. In more recent work, Hohreiter and Hahn found significant differences

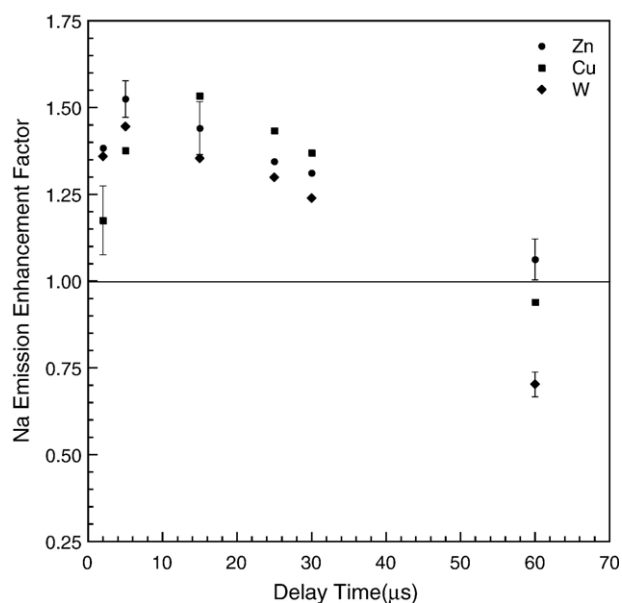


Fig. 3. Enhancement of the sodium doublet emission intensity as a function of delay time with respect to plasma initiation for sodium–copper, sodium–zinc, and sodium–tungsten containing aerosols at a 1:9 mass ratio. Data are normalized to the sodium doublet emission intensity for the pure sodium-based aerosols at each respective delay time. Representative error bars correspond to the standard deviation.

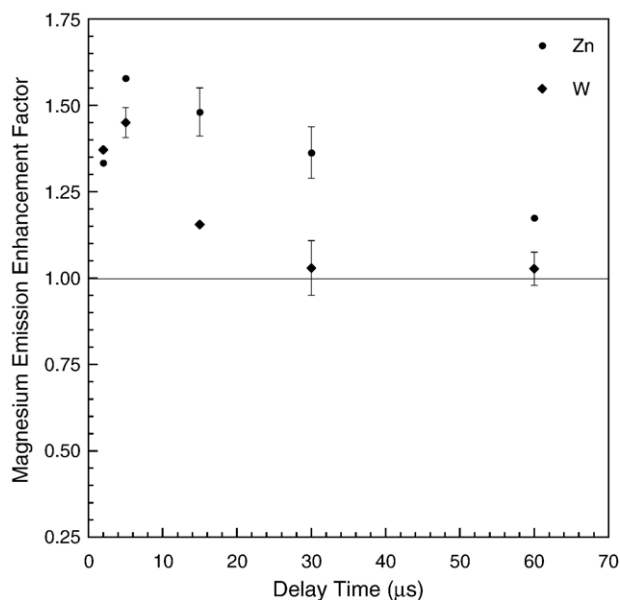


Fig. 4. Enhancement of the magnesium neutral emission intensity (285.2 nm) as a function of delay time with respect to plasma initiation for magnesium–zinc, and magnesium–tungsten containing aerosols at a 1:19 mass ratio. Data are normalized to the magnesium emission intensity for the pure magnesium-based aerosols at each respective delay time. Representative error bars correspond to the standard deviation.

between the carbon emission signal when comparing gaseous and particulate carbon sources [24]. The differences in analyte response were attributed to the preferential concentration of particulate-phase analyte within the rarefaction following plasma expansion, which was further supported by additional double-pulse laser experiments [29]. In another recent paper, Mukherjee et al. proposed an internal calibration scheme for quantitative analysis of nanoaerosols that was designed to eliminate effects due to differing plasma conditions at various analyte-dependent delay times [30]. Their approach, however, utilizes emission lines arising from the bulk plasma gases which, as discussed below, may not reflect the local environment about the aerosol particle-derived analyte. The current findings, in combination with these previous studies, suggest that fundamental changes in the analyte emission are resulting from changes in the aerosol elemental mass composition. Importantly, these changes in analyte emission have a strong temporal dependency, with the general trend being a convergence toward matrix independence with increased time following plasma initiation. For nearly all measurements reported here, the analyte enhancement factors approached unity for delays times of 60 μs , as seen in Figs. 3 and 4, with the exception being Na emission in the presence of W, which showed an actual decrease at the longest delay time. Finally, an important feature of this data set is the correlation of the enhancement results with the volatility of the concomitant element. In the LA-ICP-MS communities, there is a general view that volatility plays a role in fractionation effects. The overall trend here is an increase in the degree of analyte enhancement with increasing volatility, although such a correlation contains a degree of scatter. The role of volatility

is further elaborated on below in consideration of the additional findings.

This overall behavior may be explained in the context of recent imaging studies of single particles within laser-induced plasmas that was discussed above [3]. The fact that aerosol-derived atoms were found to be highly localized about the aerosol particle over time-scales of microseconds suggests that the analyte emission process is not governed by the volume-integrated plasma properties (i.e. bulk properties), but rather the *localized* plasma environment about the aerosol particle. As these particle-derived atoms diffuse to a length-scale approaching the overall plasma volume, which is on a time scale of some tens of microseconds, the effective plasma parameters of the aerosol-derived atoms must converge to the overall plasma parameters, at which point independence of analyte response on other concomitant species should be achieved.

Such a framework suggests that the local plasma conditions about an individual aerosol particle will differ from the bulk plasma conditions at early and intermediate times; hence differing excitation temperatures and electron densities, and consequently differing ionization fractions, will lead to perturbations in the analyte emission response. With such conditions localized to the aerosol particles, changes in aerosol mass composition can affect the degree of local plasma perturbation, giving rise to the type of matrix effect observed in the present study. To gain additional insight, more detailed spectroscopic measurements were performed using a selected magnesium–cadmium aerosol system.

3.2. Localized plasma measurements for Mg/Cd aerosol particles

Experiments were performed for solutions of 500 μg Mg/ml with an additional amount of cadmium at concentrations of 2500, 5500 and 8500 μg Cd/ml, corresponding to Mg:Cd mass ratios of 1:5, 1:11 and 1:17. The magnesium atomic emission intensity of both the ion (280.27 nm) and neutral (285.21 nm) lines were integrated. The magnesium ion peak at 280.27 nm was found to overlap with some additional spectral features (see Fig. 5) at certain delay times. The additional lines are attributed to the Mg II lines at 279.16 and 279.88 nm. Therefore, to more accurately calculate the integrated peak, the Mg emission profiles were fit to Gaussian functions (Doppler broadening), which were then used for integration. Both Lorentzian and Gaussian functions were assessed, and the Gaussian was found to produce an excellent fit. In addition, the atomic emission of the cadmium ion at 226.50 nm ($0\text{--}44,136\text{ cm}^{-1}$) and the cadmium neutral at 228.80 nm ($0\text{--}43,692\text{ cm}^{-1}$) were recorded and quantified using the full-width integrated emission peak. These measurements of Mg and Cd emission were performed over temporal delays from 2 to 40 μs , which provided emission signals for both the magnesium and cadmium ion and neutral lines with good signal-to-noise ratios. Beyond 40 μs , the intensity of the cadmium ion emission line became too weak for quantitative analysis.

Particles were collected directly on TEM grids within the LIBS sample chamber for the Mg:Cd mass ratios of 1:5 and 1:17. The collected particles were analyzed with TEM and energy dispersive

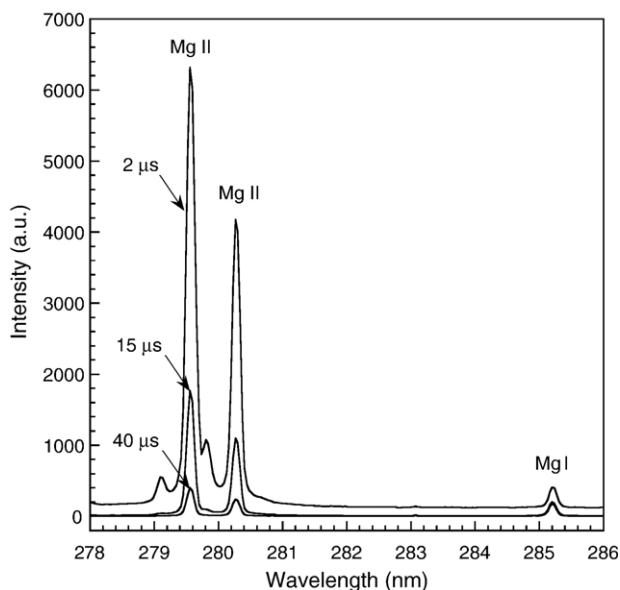


Fig. 5. Magnesium emission spectra recorded for magnesium–cadmium aerosol particles at a 1:17 mass ratio as a function of delay time. All three spectra are presented with the same intensity scale.

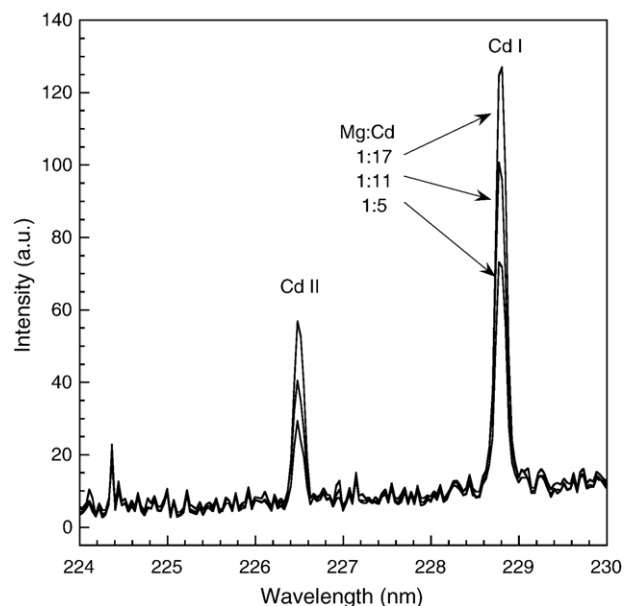


Fig. 6. Cadmium emission spectra recorded for magnesium–cadmium aerosol particles at a fixed delay of 25 μs as a function of Mg:Cd mass ratio. All three spectra are presented with the same intensity scale.

spectroscopy (EDS). No quantitative image analysis was performed, but the particle size fell primarily within the 50 to 100 nm range, and importantly, EDS revealed elemental compositions of Mg and Cd in ratios consistent with the original solution mass ratios. Overall, the TEM analysis revealed that submicron-sized aerosol particles were produced that are composed of binary mixtures of magnesium and cadmium.

An advantage of using magnesium and cadmium as analytes is the ability to observe both ion and neutral emission lines in the same spectral window. As observed in Fig. 5, the ion-to-neutral emission ratio decreases with time as the local plasma temperature and electron density change with increased plasma lifetime. However, because the ionization fraction and the overall emission intensity are coupled via Boltzmann and Saha relations, it is not possible to uniquely determine such properties from the magnesium spectral data alone. Uncoupling temperature, electron density, and ionization fraction effects is particularly difficult given the finite timescale for particle dissociation, which means that the local (i.e. centered about the aerosol particles) plasma conditions are rapidly changing as energy is absorbed by particle vaporization and ionization requirements, and additional electrons are released. To quantify such perturbations to the plasma conditions, additional spectroscopic measurements were made in the vicinity of the cadmium ion and neutral emission lines. Fig. 6 shows the spectra recorded in the vicinity of the cadmium emission lines for the three different Mg:Cd mass ratios at a fixed delay time of 25 μs . As observed in the figure, the cadmium emission signal does increase with increasing cadmium mass fraction within the aerosol particles, and as noted above, the continuum emission intensity remains identical, again demonstrating the independence of the bulk plasma continuum emission on the presence of aerosol. To quantify the emission response of the cadmium aerosol fraction, the cadmium ion-to-neutral (226.5 to 228.8) emission

ratios were calculated and are presented in Fig. 7. The cadmium ion-to-neutral ratio is observed to decrease with delay time, and significantly, the data reveal a trend of increasing rate of decay of the ion-to-neutral ratio with decreasing Mg:Cd mass ratio. Fitting an exponential decay to the three curves, the decay constants are 0.062, 0.050, 0.044 μs^{-1} for Mg:Cd ratios of 1:5, 1:11, and 1:17, respectively. This behavior is evidence of changes in the local plasma conditions surrounding the Mg–Cd particles, although

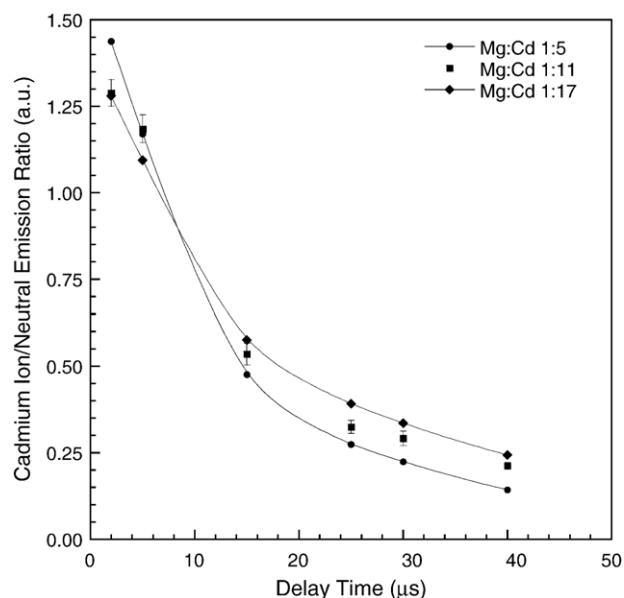


Fig. 7. Cadmium ion-to-neutral (226.5-to-228.8 nm) intensity ratios as a function of delay time with respect to plasma initiation for magnesium–cadmium mass ratios of 1:5, 1:11, and 1:17. A smooth curve is fit to the 1:5 and 1:17 mass ratio data to aid in identification of the various mass ratios. Representative error bars correspond to the standard deviation.

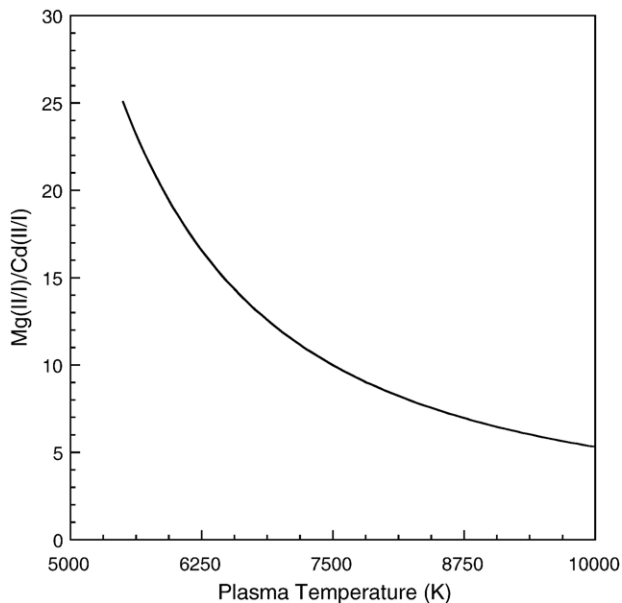


Fig. 8. Ratio of the magnesium ion-to-neutral (280.27 and 285.21 nm) intensity ratio to the cadmium ion-to-neutral (226.5-to-228.8 nm) intensity ratio as a function of plasma temperature based on the theoretical treatment of Eq. (1) [31].

quantification of the exact nature of such changes will require a combination of the magnesium and cadmium emission data.

In a recent study, Tognoni et al. proposed a unique metric for determining plasma temperature that is independent of the electron density [31]. While the ratio of ion-to-neutral emission for an individual element is a function of temperature and electron density, the ratio of the ion-to-neutral ratios of two elements eliminates electron density dependency. Assuming local thermodynamic equilibrium, a relationship between the ion-to-neutral ratios of two separate elements (here Mg and Cd) was derived as

$$\frac{R_{\text{Mg}}^{\text{II/I}}}{R_{\text{Cd}}^{\text{II/I}}} = \left(\frac{A_{ij}^{\text{II}} g_i^{\text{II}}}{A_{kl}^{\text{I}} g_k^{\text{I}}} \right)_{\text{Mg}} \left(\frac{A_{kl}^{\text{I}} g_k^{\text{I}}}{A_{ij}^{\text{II}} g_i^{\text{II}}} \right)_{\text{Cd}} \exp \left\{ \frac{[(E_i^{\text{II}} + E_{\text{ion}}) - E_k^{\text{I}}]_{\text{Mg}} - [(E_i^{\text{II}} + E_{\text{ion}}) - E_k^{\text{I}}]_{\text{Cd}}}{-k_B T} \right\} \quad (1)$$

where the following properties are defined: A_{ij} and A_{kl} are transition probabilities for the $i \rightarrow j$ (ion) and $k \rightarrow l$ (neutral) transitions, g_i and g_k are the statistical weights of the upper levels, E_i and E_k are the upper state energy levels of the ion and neutral species, respectively, E_{ion} is the ionization potential, k_B is the Boltzmann constant, and T is the plasma temperature. The subscripts refer to the elements Mg and Cd. In addition, correction terms are introduced to account for differences in instrument response at the two selected wavelengths for each element. These correction terms were set to unity, based on previous calibrations of the spectral response of our instrument. Finally, localized self-absorption is of concern if significant analyte mass is released from a single particle. Calculations

were performed using the estimated atomic concentration based on complete particle vaporization, the estimated emitting volume about the aerosol particle based on previous measurements [3], and the calculated absorption cross-sections. For all transitions, the maximum calculated turbidity was about 0.01, with the average value much less; hence all emitting volumes were considered optically thin. In the present study, Eq. (1) was implemented using the magnesium 280.27 and 285.21 nm ion and neutral lines, respectively, and the 226.5 and 228.8 nm ion and neutral cadmium lines, respectively. These lines are similar to the optimal lines suggested by Tognoni et al., with the exception of the 226.5 nm ion line, which was substituted in place of the 214.4 nm line utilized in their earlier study. However, the upper energy states of these two lines are nearly identical (44,136 vs. 46,619 cm^{-1}), and comparative calculations revealed no significant differences in the algorithm. Overall, Tognoni et al. discuss the relative errors expected with this approach, and cites values in the range of 2–4%. Using Eq. (1) for the lines detailed above, the theoretical $\text{Mg}_{\text{II}}:\text{Mg}_{\text{I}}:\text{Cd}_{\text{I}}:\text{Cd}_{\text{II}}$ ratio is presented in Fig. 8 as a function of temperature. As presented in the original publication [31], the ratio of ion-to-neutral ratios is observed to decay monotonically with increasing plasma temperature, thereby becoming a useful metric for assessment of plasma temperature independent of the plasma electron density. Using this temperature diagnostic in combination with the magnesium and cadmium emission data, the plasma temperature was calculated as a function of delay time for the three Mg:Cd mass ratios. The results are presented in Fig. 9. The data do present a degree of scatter, however, the overall trend is clearly one of an increasing temperature with increasing delay time. At the earliest times (2 to 15 μs), two of

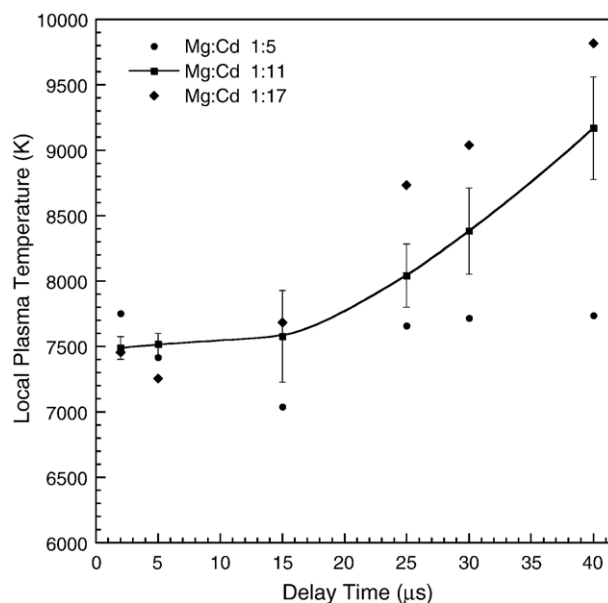


Fig. 9. Calculated local plasma temperature based on the magnesium-to-cadmium intensity ratios as a function of delay time with respect to plasma initiation based on the theoretical treatment of Eq. (1) (see Fig. 8). Representative error bars are calculated from the standard deviation of the measured experimental ratios. A smooth curve is fit to the 1:11 mass ratio data to aid in identification of the various mass ratios.

the three Mg: Cd mass ratios actually show a slight decrease in temperature, which is then followed by an increase at latter delay times. Because the overall bulk plasma temperature is decreasing with time from the onset of plasma initiation, the observed increase in local plasma temperature around the Mg–Cd particles is not perhaps so intuitive. However, if one considers finite heat transfer rates and the necessary energy to vaporize and dissociate the aerosol particles, then it is not unreasonable to assume that the local plasma temperature is initially suppressed in the vicinity of the aerosol, and therefore the local temperature will increase as heat is transferred from the hotter surrounding bulk plasma. The trends observed in the present study are consistent with recent measurements reported by Niemax et al. in an inductively-coupled plasma [32]. In that study, SiO₂ particles were found to display similar temperature profiles of an initial decrease followed by increasing temperature with plasma residence, with larger micron-sized particles showing evidence of incomplete vaporization. Additional calculations are offered below in support of these comments.

To gain insight into the vaporization and ionization of the aerosol particles, an energy balance was performed. Using the Mg and Cd mass fractions contained within an average aerosol particle size of 75 nm (estimated from the TEM analysis), the total particle mass is about 0.5 fg. This mass was then used in combination with the ionization and heat of vaporization energies (weighted average based on the particle composition) to estimate the total energy required to dissociate and ionize (50% ionization fraction) the aerosol particle, which yielded a value of 8×10^{-12} J. A region of plasma volume surrounding the particle was then coupled to supply this energy to the particle, and the corresponding reduction in temperature was calculated using the mass within this volume and the specific heat. The plasma specific heat was assumed equal to 10 kJ/kg K at an average temperature of 10,000 K based on reported calculations [33]. Using a plasma volume equal to a diameter of 500 nm (about particle 6 diameters), these calculations predict a temperature drop of 7700 K. Clearly such calculations contain a number of assumptions and approximations, but nonetheless, are consistent with the concept of a localized perturbation of the plasma temperature. Furthermore, the relative effects of heat and mass transfer may be assessed in terms of the Lewis number (α/D), which is a dimensionless parameter that compares the thermal diffusivity ($\alpha = k/\rho c$) to the mass diffusion coefficient. Once again using the published data for the thermal conductivity [33], and our previously measured value of the diffusion coefficient for calcium atoms ($D = 0.04$ m²/s), the Lewis number was calculated to be 0.25. While approximations are inherent in this calculation, such a near-unity value fully supports the concept of finite time-scales for both heat and mass transfer, which is consistent with our previously measured rates of diffusion [3], and our current results of localized plasma temperature perturbations on the order of tens of microseconds.

Given the temporal dependence of the problem due to finite diffusion timescales, the role of volatility can be considered further. The coupling of particle-derived mass to the local plasma perturbations is diminished with time as discussed above. Therefore, more volatile elements may enter the plasma earlier, leading to greater localized matrix effects, while less

volatile elements will shift the vaporization rate to longer timescales where the overall effect is somewhat mitigated. Such comments may be considered analogous to the role of volatility in LA-ICP-MS, where competition between transport toward the MS skimmer and radial diffusion may play important roles in matrix effects. This framework is consistent with the overall trends observed in the Figs. 3 and 4 data regarding the effect of volatility of the added mass.

In summary, the current results provide additional insight into the role of plasma–particle interactions pursuant to quantitative aerosol analysis with laser-induced breakdown spectroscopy. Based on recent studies by our group and others, the current picture that is emerging concerns a complex interaction between the plasma gases and the aerosol particle, during which the finite time-scales of particle dissociation, and heat and mass transfer are fundamental processes. The finding that the analyte emission derived from aerosol particles is affected by the presence of concomitant elemental fractions, as observed with the sodium and magnesium containing aerosol particles, is of significant importance to the LIBS community. Such findings are direct evidence of a matrix effect for aerosol particles, due primarily to perturbations in the localized plasma properties. However, such perturbations are minimized at longer plasma delay times; hence quantitative analysis should be performed with careful attention given to the temporal plasma evolution. In the larger analytical community, the effect of localized conditions about the individual particles is also relevant to the ICP-MS and notably the LA-ICP-MS communities, where such effects are coming under increasing scrutiny with regard to the issues of elemental fractionation and matrix effects. Important next steps are a clear understanding of the exact mechanisms associated with analyte emission perturbations.

Acknowledgements

This work was supported in part by the National Science Foundation through grant CTS-0317410. The authors express our gratitude to Elisabetta Tognoni for providing an advance copy of her theoretical framework for temperature analysis, to Prof. Kay Niemax for useful feedback and discussions regarding their recent findings presented at the European Workshop on Laser Ablation, to Prof. Detlef Gunther for sharing his insight on the roles of analyte transport in LA-ICP-MS, and to Prof. Nico Omenetto for assistance with the optical density calculations.

References

- [1] L.J. Radziemski, From laser to LIBS, the path of technology development, *Spectrochim. Acta Part B* 57 (2002) 1109–1113.
- [2] J.D. Winefordner, I.B. Gornushkin, T. Corell, E. Gibb, B.W. Smith, N. Omenetto, Comparing several atomic spectrometric methods to the super stars: special emphasis on laser induced breakdown spectrometry, LIBS, a future super star, *J. Anal. At. Spectrom.* 19 (2004) 1061–1083.
- [3] V. Hohreiter, D.W. Hahn, Plasma–particle interactions in a laser-induced plasma: implications for laser-induced breakdown spectroscopy, *Anal. Chem.* 78 (2006) 1509–1514.
- [4] Z. Whang, B. Hattendorf, D. Gunther, Analyte response in laser ablation inductively coupled plasma mass spectrometry, *J. Am. Soc. Mass Spectrom.* 17 (2006) 641–651.

- [5] M. Guillon, D. Gunther, Effect of particle size distribution on ICP-induced elemental fractionation in laser ablation-inductively coupled plasma-mass spectrometry, *J. Anal. At. Spectrom.* 17 (2002) 831–837.
- [6] C. Chaleard, P. Mauchien, N. Andre, J. Uebbing, J.L. Lacour, C. Geertsen, Correlation of matrix effects in quantitative elemental analysis with laser ablation optical emission spectrometry, *J. Anal. At. Spectrom.* 12 (1997) 183–188.
- [7] J.M. Mermet, Revisitation of the matrix effects in inductively coupled plasma atomic emission spectrometry: the key role of the spray chamber, *J. Anal. At. Spectrom.* 13 (1998) 419–422.
- [8] D. Gunther, Laser-ablation inductively-coupled plasma mass spectrometry, *Anal. Bioanal. Chem.* 372 (2002) 31–32.
- [9] J. Koch, H. Lindner, A.V. Bohlen, R. Heregenroder, K. Neimax, Elemental fractionation of dielectric aerosols produced by near-infrared femtosecond laser ablation of silicate glasses, *J. Anal. At. Spectrom.* 20 (2005) 901–906.
- [10] J. Koch, A.V. Bohlen, R. Heregenroder, K. Neimax, Particle size distributions and compositions of aerosols produced by near-IR femto- and nanosecond laser ablation of brass, *J. Anal. At. Spectrom.* 19 (2004) 267–272.
- [11] G. Rezaaiyaan, J.W. Olesik, G.M. Hieftje, Interferences in low-flow, low-power inductively coupled plasma, *Spectrochim. Acta Part B* 40 (1985) 73–83.
- [12] K. O'Hanlon, L. Ebdon, M. Foulkes, Effect of easily ionisable elements on the mass transport efficiency of solutions and slurries used in plasma emission spectrometry, *J. Anal. At. Spectrom.* 12 (1997) 329–331.
- [13] R. Russo, X. Mao, J.J. Gonzalez, S.S. Mao, Femtosecond laser ablation ICP-MS, *J. Anal. At. Spectrom.* 17 (2002) 1072–1075.
- [14] R.E. Russo, X.L. Mao, O.V. Borisov, H.C. Liu, Influence of wavelength on fractionation in laser ablation ICP-MS, *J. Anal. At. Spectrom.* 15 (2000) 1115–1120.
- [15] D. Bleiner, D. Gunther, Theoretical description and experimental observation of aerosol transport processes in laser ablation inductively coupled plasma mass spectrometry, *J. Anal. At. Spectrom.* 16 (2001) 449–456.
- [16] D. Gunther, R. Frischknecht, C.A. Heinrich, H.J. Kahlert, Capabilities of an argon fluoride 193 nm excimer laser for laser ablation inductively coupled plasma mass spectrometry microanalysis of geological materials, *J. Anal. At. Spectrom.* 12 (1997) 939–944.
- [17] H. Lindner, J. Koch, K. Niemax, Production of ultrafine particles by nanosecond laser sampling using orthogonal prepulse laser breakdown, *Anal. Chem.* 77 (2005) 7528–7533.
- [18] R.S. Houk, N. Praphairaksit, Dissociation of polyatomic ions in the inductively coupled plasma, *Spectrochim. Acta Part B* 56 (2001) 1069–1096.
- [19] D.A. Wilson, G.H. Vickers, G.M. Hieftje, Ionization temperatures in the inductively coupled plasma determined by mass-spectrometry, *Appl. Spectrosc.* 41 (1987) 875–880.
- [20] S.A. Lehn, K.A. Warner, M. Huang, G.M. Hieftje, Effect of an inductively coupled plasma mass spectrometry sampler interface on electron temperature, electron number density, gas-kinetic temperature and analyte emission intensity upstream in the plasma, *Spectrochim. Acta Part B* 57 (2002) 1739–1751.
- [21] B. Budic, Matrix effects in inductively coupled plasma atomic spectrometry using an ultrasonic nebulizer, *J. Anal. At. Spectrom.* 13 (1998) 869–874.
- [22] J.W. Olesik, Investigating the fate of individual sample droplet in inductively coupled plasmas, *App. Spectrosc.* 1 (1997).
- [23] V. Hohreiter, A. Ball, D.W. Hahn, Effects of aerosols and laser cavity seeding on spectral and temporal stability of laser-induced plasmas: application to LIBS, *J. Anal. At. Spectrom.* 19 (2004) 1289–1294.
- [24] V. Hohreiter, D.W. Hahn, Calibration effects for laser-induced breakdown spectroscopy of gaseous sample streams: analyte response of gaseous phase species vs. solid phase species, *Anal. Chem.* 77 (2005) 1118–1124.
- [25] D.W. Hahn, J.E. Carranza, G.R. Arsenault, H.A. Johnsen, K.R. Hencken, Aerosol generation system for development and calibration of laser-induced breakdown spectroscopy instrumentation, *Rev. of Sci. Instrum.* 72 (2001) 3706–3713.
- [26] D.W. Hahn, M.M. Lunden, Detection and analysis of aerosol particles by laser-induced breakdown spectroscopy, *Aero. Sci. and Tech.* 33 (2000) 30–48.
- [27] D.W. Hahn, W.L. Flower, K.R. Hencken, Discrete particle detection and metal emissions monitoring using laser-induced breakdown spectroscopy, *App. Spec.* 51 (1997) 1836–1844.
- [28] M. Essien, L.J. Radziemski, J. Sneddon, Detection of cadmium, lead and zinc by laser-induced breakdown spectroscopy, *J. Anal. Atomic Spectrom.* 3 (1988) 985–988.
- [29] B.C. Windom, P.K. Diwakar, D.W. Hahn, Dual-pulse LIBS for analysis of gaseous and aerosol systems: plasma-analyte interactions, *Spectrochim. Acta Part B* 61 (2002) 788–796.
- [30] D. Mukherjee, A. Rai, M.R. Zachariah, Quantitative laser-induced breakdown spectroscopy for aerosols via internal calibration: application to the oxidative coatings of aluminum nanoparticles, *Aerosol Sci.* 37 (2006) 677–695.
- [31] E. Tognoni, M. Hidalgo, A. Canals, G. Cristoforetti, S. Legnaioli, A. Salvetti, V. Palleschi, Combination of the ionic-to-atomic line intensity ratios from two test elements for the diagnostic of plasma temperature and electron number density in Inductively Coupled Plasma Atomic Emission Spectroscopy, *Spectrochim. Acta Part B* 62 (2007) 435–443.
- [32] M. Miclea, I. Exius, H. Lindner, C. Garcia, K. Niemax, Characterization of Laser Produced Particles by ICP-OES, Presented at the 8th European Workshop on Laser Ablation, Zurich, July 19–21, 2006.
- [33] J. Aubreton, M.F. Elchinger, P. Fauchias, New method to calculate thermodynamic and transport properties of a multi-temperature plasma: application to N₂ plasma, *Plasma Chem. And Plasma Processing* 18 (1998) 1–27.